One-dimensional modelling of DBDs in NeXe mixtures for excimer lamps

A Belasri, K Khodja, S Bendella, Z Harrache

One–dimensional modeling of DBDs in Ne–Xe mixtures for excimer lamps

A Belasri[1], K Khodja[1], S Bendella[1] and Z Harrache[2]

[1] Laboratoire de Physique des Plasmas, Matériaux Conducteurs et leurs Applications, Université des Sciences et de la Technologie d'Oran El-Mnaour B.P.1505, 31000 Oran, Algérie
[2] Grupo de Espectroscopia de Plasmas, Universidad de Cordoba, Edificio C-2, 14071 Cordoba, Spain.

Abstract

Dielectric barrier discharges (DBDs) are a promising technology for high-intensity sources of specific UV and VUV radiation. In this work, the microdischarge dynamics in DBDs for Ne–Xe mixtures under the close conditions of excimer lamp working has been investigated. The computer model including the cathode fall, the positive column and the dielectric is composed of two coupled sub-models. The first submodel describes the electrical properties of the discharge and is based on a fluid, two-moments description of electron and ion transport coupled with Poisson's equation during the discharge pulse. The second submodel, based on three main modules: a plasma chemistry module, a circuit module and a Boltzmann equation module, with source terms deduced from the electric model, describes the time variations of charged and excited species concentrations and the UV photon emission. The use of the present description allows a good resolution near the sheath at high pressure and it predicts correctly the waveform of the discharge behavior. The effects of operation voltage, dielectric capacitance, gas mixture composition, gas pressure, as well as the secondary electron emission by ion at the cathode on the discharge characteristics and the 173 nm photon generation have been investigated and discussed.

Key words: DBDs; Ne–Xe mixtures; Excimer lamp; Sheath; Modeling.

PACS: 51.50.+v ; 52.20.-j ; 52.80.-s ; 82.33.Xj.

1. Introduction

The dielectric barrier discharges are more and more used in technology for generating non-local thermal equilibrium (non–LTE) plasmas near atmospheric pressure [1–4], in particularly for ozone generation [4–6], surface treatment and thin film deposition [7, 8], flue gas treatment [9, 10], pollution control [11, 12], laser pumping [13–15] and production of ultra-violet (UV) and vacuum ultra-violet (VUV) radiation [4, 16–20]. The DBDs are used due to their simplicity, stability, low cost, high power, and easy maintenance. In the last decade, excimer lamps excited by dielectric barrier discharges have received much attention by scientific communities. In particularly, because they provide an efficient scheme for generating incoherent spontaneous UV and VUV

excimer radiation with a long lifetime, the working mixture does not have a contact with metal electrodes and the current is limited by the dielectric [21–25]. Originally proposed by Eliasson and Kogelschatz [16], excimer formation in DBDs have a large potential of applications, such us UV biological sterilization, photochemical surface treatment, pollution control, plasma display panels, ozone generation, microlithography, photolytic vapor deposition and material deposition in microelectronics [26–34]. During the last few years DBDs UV sources have been investigated using many different excited species, including rare gas excimers (such as Kr_2^*, and Xe_2^*), molecular rare gas halide excimers (such as $ArCl^*$, $KrCl^*$, $XeCl^*$ and XeBr), and halogen dimmers (such as Cl_2^*, F_2^*, and Br_2^*), with high efficiency (>10%) and where a wide range of UV spectrum can be covered [16, 17, 35–40]. In particularly, excimer and exciplex lamps are mercury free systems and ecologically friendly, and therefore they are predestined for the lighting industry [41–45]. In order to optimize the discharge luminance efficiency, most experimental and theoretical works have been realized in DBD's for excilamps [22–24, 46–55]. Several models on DBDs for excilamps were developed during this last decade. The model used by Oda *et al* [23, 47] bases itself on the resolution of the continuity equations of electrons and ions, the energy conservation equation and Poisson's equation. Liu and Neiger [48] have developed a dynamic electrical model. The model used by Carman *et al* [22, 49, 50] analyzes the spatiotemporal evolution of species populations and electrical parameters. Also, in order to investigate the spatiotemporal characteristics of the short-pulsed DBDs in pure xenon, a 1D and 2D fluid models was used by Bogdanov *et al* [24, 51]. S. Belezenai *et al* in Ref. [46], reported that in xenon discharge lamp most power is deposited in the high field region in the vicinity of the dielectric barriers, about 21% of the total input power was used by ion heating. X. Jing-zhon *et al* [56] have investigated the influence of the gas temperature in DBDs on the excimer emission.

In this work, computer model including the sheath, the dielectric and the positive column has been developed to investigate the microdischarge dynamics in dielectric barrier discharges operating in Ne–Xe mixtures. The context of this study is the modelling of the DBDs with a reasoned approach for controlling VUV emission in excimer lamp. The model predicts the optimal operating conditions and describes the electrical and chemical properties of the excimer lamp. We present in Sec. 2 an overview of the physical and the kinetic models. In Sec. 3, the salient numerical results are presented and discussed. The conclusion of the present work is summarized in Sec. 4.

2. Model

The computer model including the cathode fall, the positive column and the dielectric was based on two coupled sub-models as used in Refs. [57, 58]. In this model, the space gradients are supposed to exist only in the cathode sheath described by the one−dimensional fluid model, and the positive column which is supposed to be spatially uniform was studied by a zero−dimensional model. The gap length d is considered to be equal to $d_{cr}+ d_{plas}$, where d_{cr} is the length of cathode sheath limited by the cathode and the plasma and d_{plas} is the plasma length (see Figure 1). In order to have a good numerical resolution the length of the cathode sheath region described with the one-dimensional model is typically d_{cr}=3 mm in the calculation presented below. This region includes the (time-varying) sheath and a small part of positive column plasma. The boundary condition on the plasma side of the cathode region ($x=d_{rc}$) is such that the charged-particle density gradients are zero. This discharge region is supposed to be in series with the rest of the plasma (described with the zero-dimensional model). For the considered operating conditions of excimer lamp in this work, the maximum value of the sheath length d_s (the sheath end, i.e., the sheath-plasma boundary defined here as the point where the electron density become larger than half the ion density) reached before the plasma formation is about 2 mm, which will be small to cathode region length, and then to the gap distance ($d_s<d_{cr}<d$). In the frame of this study, the cathode region length d_{cr} is supposed equal to 3 mm (region studied with the 1D model) which will be greater than the maximum value of the sheath length d_s reached before the plasma formation under different lamp operation conditions. The applied voltage through the discharge is given by:

$$V_{ap}(t)= V_D(t)+ V_{cr}(t)+ V_{plas}(t) \quad (1)$$

where $V_{plas}(t)$, $V_D(t)$ and $V_{cr}(t)=V(d_{cr}, t)$ are the voltage across the positive column, the dielectric and the cathode region respectively for a given time t. The relation between the current I_{cr} and the voltage V_{cr} in the cathode region is described by the current equation:

$$I_{cr}(t) = - \varepsilon_0 \frac{A}{d_{cr}} \frac{\partial V_{cr}}{\partial t} + \frac{A}{d_{cr}} \int_0^{d_{cr}} \left[J_e(x, t)+ J_p(x, t)\right] dx \quad (2)$$

where A represents the electrode area, and $J_e(x, t)$ and $J_p(x, t)$ are, the electron and ion current density respectively for a given position x and time t.

The zero−dimensional model consists of three main modules: a plasma chemistry module, a circuit module and a Boltzmann equation module. The plasma chemistry module constructs differential equations for the evolution of the density of species. The system of equations describing the dielectric, the positive column and the cathode region are solved in two steps as follows; for a given voltage V_{cr} across the cathode region at a time t, the plasma kinetic equations coupled with the dielectric equation are solved with the classical GEAR method

[59] between the instants t and t+dt. Taking I_{cr} in equation (2) from the above calculation ($I_{cr}=I_{plas}$) at time (t+dt), where I_{plas} is the plasma current calculated in the positive column, the one-dimensional fluid equations are integrated in space ($0<x<d_{cr}$) and time between t and (t+dt).

For the kinetic scheme, we consider the Ne–Xe mixture used in Refs. [60, 61], including the charged particles of electrons (e), atomic ions (Xe^+, Ne^+), molecular ions (Ne_2^+, Xe_2^+, $NeXe^+$), the excited atomic and molecular species of $Xe^*(\ ^3p_1)$, $Xe^*(\ ^3p_2)$, Xe^{**}, $Xe_2^*(O_u^+)$, $Xe_2^*(\ ^3\Sigma_u^+)$, $Xe_2^*(\ ^1\Sigma_u^+)$, $Ne^*$and the photonic species hν (173 nm), hν (147 nm) and hν (150 nm) (see Table 1). The bibliographic research on Ne–Xe gas mixture shows that this kinetic scheme constitutes the basis of the set of models used for the description of plasma display panels (PDPs) [60, 61, 72], excimer lamps and lasers. The transport coefficients and the electronic collision frequencies which depend on the reduced electric field E/N are therefore precalculated and tabulated by solving the steady state, homogeneous electron Boltzmann equation in the considered gas mixture, using Bolsig+ software [62].

The one-dimensionnel fluid model, based on two-moments description of electron and ion transport coupled with Poisson's equation during the discharge pulse, describes the space and time variations of the electron and ion densities, the electric field and the current density. The positive column model describes the time variations of charged and excited species concentrations and of the UV photon emission.

3. Results and discussion

3.1. Input conditions

The DBDs lamp parameters and operating conditions used in the present work are shown in Table 2. These parameters of the discharge configuration and operating conditions are chosen, in the range order of that used in recent experimental and theoretical works [21-24, 47-51, 53] on excimer lamp, in the objective to have a spatially uniformity of the plasma across the discharge area and a high lamp efficiency.

3.2. Discharge behavior

In this paragraph, we illustrate the formation and the quenching of a single discharge in a mixture of 10% xenon in neon, with a total pressure of p_r = 400 Torr, the applied voltage is equal to 2 kV, and the capacity of the dielectric layer above each electrode is 460 pF/cm^2 (the equivalent capacitance of the two layers, C_{diel}, is therefore 230 pF/cm^2). In this work, a secondary emission coefficient [24, 47, 60, 61, 74] of 0.25 has been assumed for neon ions. Usually, in DBD's configuration for display panels or lamps a MgO thin film is deposited above the dielectric layers in order to protect the dielectric layers, and decrease the breakdown voltage

due to the relatively large value of the secondary electron emission coefficient of MgO bombardment by neon ions. Note that the value of the secondary emission coefficient due to xenon ions is about ten times smaller to that of neon ions

3.2.1. Current and voltage across the gap

Figure 2 shows, the time variations of the voltage across the positive column V_{plas}, the voltage across the cathode region V_{cr}, the voltage across the dielectric V_D, and the current. It seems, that at any time during the discharge pulse, the voltage equality $V_{ap} = V_{cr} + V_{plas} + V_D$ is realized, and the transition from capacitive to resistive behaviour of the sheath is observed by a voltage increase and decrease across the cathode region to reach the desired operating point. This figure shows also, that the discharge is initiated in the gap after a delay time of about 20 ns. The current density increases this time and reaches a peak value of 2.7 A/cm^2 at the instant t= 243 ns. The current density then decreases rapidly to reach a low value at the end of the discharge pulse. The decrease of the current density is due to the charging of the dielectric layers by electrons and ions generated in the discharge volume and flowing to the walls. The voltage induced by the charging of the dielectric layers opposes the applied voltage and increases to reaches a maximum value at the end of the pulse. This value of V_D is sufficient to ensure the next discharge.

3.2.2. Electric field and charged particle densities

Figure 3 illustrates the spatial distribution of the electric field, electron and ion densities in the cathode region at six different times of the discharge pulse. These times (t = 5, 10, 19.7, 156, 243 and 940 ns) are indicated on the current curve in figure 2. During the first pulse period, the electric field is spatially uniform, and the electrons move towards the anode (the cathode is defined at the position x=0), inducing gas ionization. During this time the electrons have drifted a distance of about 1.3 mm, which is the maximum sheath length. After about 20 ns, which is the time for breakdown, the plasma is formed and an ionic space charge is created near the cathode, accompanied by a field increase to high values. These large values lead to high ionization in front of the sheath, followed by a rapid motion of the sheath–plasma boundary toward the cathode. Two discharge regions are distinguished. At first, a cathode fall region exists where the electric field drops drastically from a maximum value of about 1.6×10^5 V/cm at the moment of the peak current (t=243 ns), also the ion density reaches its largest value of 3.7×10^{13} cm^{-3} and the sheath length is about 0.005 cm. Secondly, a positive column plasma is observed characterized by quasi neutrality and a very low value of the electric field.

3.2.3. Species concentrations and UV photon emission

The temporal evolution of the Ne–Xe mixture concentrations, obtained with the kinetic model, is presented in figures 4(*a*)–(*c*). These figures show that after the breakdown phase, a fast growth of excited and charged species densities are noticed. The dominant ions in positive column are Xe^+ and Xe_2^+, as appeared in figure 4(*a*), which represents the time variations of the Xe^+, Ne^+, Xe_2^+, Ne_2^+, and $NeXe^+$ concentrations, together with the electron density n_e. The time variations of the excited atoms and molecules $Xe^*(\,^3P_2)$, $Xe^*(\,^3P_1)$, Xe^{**}, Ne^*, $Xe_2^*(\,^3\Sigma_u^+)$, $Xe_2^*(\,^1\Sigma_u^+)$, and $Xe_2^*(O_u)$ are plotted in figure 4(*b*). The metastable state $Xe^*(\,^3P_2)$ reaches a maximal value of 1.58×10^{14} cm^{-3}, then decreases much slower during the discharge pulse, while the resonant state $Xe^*(\,^3P_1)$ reaches a maximum of 7.5×10^{13} cm^{-3} and decreases rapidly. Note that the excited molecular state $Xe_2^*(\,^3\Sigma_u^+)$ density has a maximum of 3.4×10^{11} cm^{-3} and follows closely the time variation of $Xe^*(\,^3P_2)$. However, the time variations of $Xe_2^*(\,^1\Sigma_u^+)$ and $Xe_2^*(O_u)$ concentrations are almost identical to those of $Xe^*(\,^3P_1)$ with maximum values of 1.5×10^{11} cm^{-3} and 2×10^{11} cm^{-3} respectively. This variation of the atomic and molecular excited species is confirmed in Ref. [60]. It is due to the kinetic scheme used (see Table 1). In the Xe DBDs plasma, VUV emission is generated via the radiative decay of the four excited xenon states: the $Xe^*(\,^3P_1)$ resonance level (147 nm), the $Xe_2^*(O_u)$ vibrationally excited level (150 nm) and the excimers $Xe_2^*(\,^3\Sigma_u^+)$, $Xe_2^*(\,^1\Sigma_u^+)$, both at 173 nm. The time variation of the photonic species, hν (173 nm), hν (147 nm) and hν (150 nm), was shown in figure 4(*c*).

3.3. Parametric studies

The dielectric discharge lamps convert electrical energy into radiation by transforming electrical energy into kinetic energy of moving electrons, which in turn is converted into electromagnetical radiation as a result of some kind of collision process with atoms of gas. The luminous efficacy of the excimer lamp is determined by the vacuum ultraviolet VUV photon emission which transfers into visible light by the phosphor. However it is interesting to look at how the energy gained by electrons and ions from the electric field is dissipated inside the cell. Recently, several experimental and theoretical works have focused on the lamp efficiency [4, 21-24, 46, 47, 49-51, 60, 61], and it has been shown that the efficiency of excimer lamps is directly dependent on the electron energy deposition in xenon excitation, and can be drastically increased in a pulsed regime. It seems possible to modify the power deposition in the plasma by varying external discharge parameters such as the amplitude and the rise time of the applied voltage, and to modify the plasma composition by changing the gas mixture and pressure. In this subsection, we discuss the dependence of VUV photon generation and the DBDs behaviour on

the dielectric properties, the gas mixture composition, the gas mixture total pressure, the applied voltage and the secondary electron emission process.

3.3.1. Effect of the applied voltage

In order to study the interactions between the power supply and the lamp, we illustrate in figure 5(*a*), the time variations of the discharge current pulse, under the same conditions of subsection 3.2 and for three value of applied voltage V_{ap} = 1.5, 2 and 3 kV. In this figure, it appears clearly the strong effect of the applied voltage on the breakdown time and the current peak. It is instructive to look at the time variation of the electric field at the cathode, for different values of the applied voltage. The time variation of the cathode electric field as plotted in figure 5(*b*) is similar to that of the current discharge. For the three values of applied voltage 1.5, 2 and 3 kV, the peak of the electric field reaches respectively the following values 4.5×10^5, 1.6×10^5 and 8.8×10^4 V/cm. These large values of electric field in the vicinity of the dielectric will lead to a large power deposition [46, 60], however a significant ion heating will be noticed which will probably limit the lamp efficiency. Figure 6 investigates the effect of varying the applied voltage amplitude V_{ap} on photon hν (173 nm) emission in DBDs. It is known that increasing V_{ap} increases the light emission due largely to increasing energy deposition, and the most of the energy dissipated in exciting xenon is used in the VUV production.

3.3.2. Effect of the Xe concentration

In order to see how the electrical and chemical characteristics of the plasma can be affected by xenon concentration in Ne–Xe gas mixtures, it is interesting to look at the time variations of the discharge current and the photon hν (173 nm) density, as displayed in figures 7(*a*)–(*b*) respectively, for three concentrations of xenon in neon and an applied voltage of 3 kV at a fixed pressure of 400 Torr. We can see clearly that, the generation of 173 nm photons increases with the increasing of the xenon mole fraction in the mixture [21, 22, 73–75]. However for low concentrations of xenon, the discharge current is higher because an important fraction of power deposition goes into producing ionization. Figure 8 illustrates the effect of the xenon concentration on the secondary electron current due to photon impact on the cathode $J_{e,\,h\nu}$. The photoelectron current [49, 57, 58, 63] is obtained by the relation:

$$J_{e,\,h\nu}=\frac{1}{2}\, e\, Q\, d\, S_{h\nu}$$

where Q is the quantum efficiency for photon electron generation, which represents the number of electrons released from the electrode per incident photon. In this work we have assumed a quantum efficiency of $Q=10^{-2}$, which represents an upper limit for the 173 nm incident photons on a 4 eV work-function cathode material. The production rate $S_{h\nu}$ of the 173 nm photons has been obtained from the density of excited molecule Xe_2^*.

3.3.3. Effect of pressure

We also investigated the consequences of gas mixture total pressure on the discharge current, the photon generation and excited species under the same conditions of subsection 3.2, in figures 9, 10, and 11. As pressure increases, the discharge sustaining voltage becomes larger. Then for a constant value of applied voltage V_{ap}= 2 kV, the current peak will be decreased when the gas pressure increases (see Figure 9). The emissions of the three photons (147 nm, 150 nm and 173 nm) increase with increasing gas pressure due to higher gas density resulting in more UV emission. However the efficiency of 173 nm photon generation is high at high-pressures because the three body collisions are more efficient to generate $Xe_2^*(\,^3\Sigma_u^+)$ [22] as shown in figures 10(*a*)–(*b*). Figures 11(*a*)–(*b*) report the effect of the total pressure on the time variation of the metastable state $Xe^*(\,^3P_2)$ and the resonant state $Xe^*(\,^3P_1)$ respectively. We see that the density of the metastable state decreases with the increasing of the gas pressure. This diminution in metastable density is due in part to its conversion to $Xe_2^*(^3\Sigma_u^+)$, collision with the fundamental state of xenon [21, 22, 60]. However, we can expect that the reaction R3 (see Table 1) can also contribute to this diminution as the pressure increasing induces a decrease in the plasma electric field.

3.3.4. Effect of dielectric capacitance

The consequences of the dielectric capacitance on the deposed power and the 173 photon generation, for three values of C_{diel} =100, 230, 400 pF/cm^2 and under the same conditions of subsection 3.2, are shown in figures 12(*a*)–(*b*). With a larger dielectric capacitance, more current is required to charge the dielectric. Therefore, more energy is deposited in the plasma and the corresponding photon fluxes are larger (Figure 12(*b*)). Figure 12(*a*) shows also, that the power density has a similar profile as the discharge current pulse and the time to breakdown is not affected by the presence of the dielectric.

3.3.5. Effect of the secondary electron emission

The presence of the cathode sheath in series with the plasma of the positive column can have a big influence on the evolution of the voltage, current, and chemical kinetics in the plasma. In order to illustrate this effect, we plotted in figure 13, the time evolution of the discharge current, plasma voltage and the dielectric voltage when the sheath is not considered. This result has been obtained by solving the zero-dimensional model plasma kinetic equation described in the model section (see Table 1) for the case when the positive column has a distance equal to the total gap distance (i.e., without considering the cathode region) coupled with the dielectric equation and under the same conditions of subsection 3.2. We see that the pulse duration is about 200 ns and the discharge current density has a peak of 23 A/cm^2. We report on figures 14(*a*)–(*b*), the time variation during the

discharge pulse of the current and the 173 nm photon density, obtained with the complete one-dimensional model, including positive column, cathode region, and the circuit equations, for two values of secondary emission coefficient $\gamma = 0.25$ and 0.1. We see clearly from these figures, that the plasma electrical characteristics and kinetics are strongly affected by the presence of this cathode region; however, the presence of the sheath cannot be neglected in theoretical models developed to study the DBDs characteristics. We note that the current of the discharge and the 173 nm photon production increase with the large values of secondary emission coefficient at the cathode.

4. Conclusion

The fundamental objective of the dielectric discharge lamps is to convert electrical energy into radiation by transforming electrical energy into kinetic energy of moving electrons, which in turn is converted into VUV radiation. This work presents a reasoned approach to deliver electric energy into a dielectric barrier discharge excimer lamp, with the aim of controlling its VUV emission. The computer model including the cathode fall, the positive column and the dielectric, describes under the same conditions of excimer lamp working, the spatial and time variations of the electrical and chemical discharges properties during the pulse; current, electric field, voltage across the micro-discharge, charged and excited species concentrations and the VUV photon emission. The results discuss the microdischarge dynamics and the optimization of discharge conditions for excimer lamp and photon generation. The efficiency of VUV photon generation in DBDs depends on the dielectric properties, gas mixture composition, gas mixture pressure, applied voltage and the sheath via secondary electron emission at the cathode. The increase of the applied voltage, xenon concentration, gas pressure, and the dielectric capacitance induces an increasing in 173 nm photon generation. From the result of the secondary electron emission effects on the discharge behavior, one can deduce that taking account of the sheath is indispensable to have a realistic approach, in theoretical models developed to study DBD's for excimer lamp. Finally, the results of this work can be considered as important design data of excimer lamps for practical applications.

Acknowledgments

This work was funded by the Algerian Ministry of Education and Research. Z. H. is grateful to Professor M.D. Calzada for the kind hospitality during the realization of this work.

References

[1] Kogelschatz U, B.Elliasson B and Egli W 1999 *Pure & Appl. Chem*. **71** 1819.

[2] Eliasson B and Kogelschatz U 1991 *IEEE. Trans. Plasma Sci*. **19** 309.

[3] Elliasson B, Egli W and Kogelschatz U 1994 *Pure & Appl. Chem*. **66** 1275.

[4] Kogelschatz U 2003 *Plasma Chemistry and Plasma Processing* **23** 1.

[5] Siemens W 1857 *Ann. Chim. Phys*. **102** 66.

[6] Eliasson B, Hirth M and Kogelschatz U 1987 *J. Phys. D Appl. Phys.* **20** 1421.

[7] Kanazawa S, Kogoma M, Moriwaki T and Okazaki S 1988 *J. Phys. D: Appl. Phys*. **21** 838.

[8] Massines F, Mayoux C, Messaoudi R, Rabehi A and Segur P 1992 *Proc. of the International Conference on Gas Discharges and Their Applications*, Swansea (UK), p. 730.

[9] Chang M B, Balbach J H, Rood M J and Kushner M J 1991 *J. Appl. Phys.* **69** 4409.

[10] Chang M B, Kushner M J and Rood M J 1992 *Plasma Chemistry and Plasma Processing* **12** 565.

[11] Clothiaux E J, Koropchak J A and Moore R R 1984 *Plasma Chemistry and Plasma Processing* **4** 15.

[12] Storch D G and M.J. Kushner M J 1993 *J. Appl. Phys*. **73** 51.

[13] Yagi S and Tabata N 1981 *IEEE/OSA Conference on Lasers and Electro-Opt.*, Washington, D. C., p. 22.

[14] Yasui K, Kuzumoto M, Ogawa S, Tanaka M and Yagi S 1989 *IEEE. J. Quantum Electron* **25** 836.

[15] Takenaka Y, Kuzumoto M, Yasui K, Yagi S and Tagashira M 1991 *IEEE. J. Quantum Electron* **27** 2482.

[16] Eliasson B and Kogelschatz U 1988 *Appl. Phys.* B **46** 299.

[17] Erofeev M V and Tarasenko V F 2006 *J. Phys. D: Appl. Phys*. **39** 3609.

[18] Kogelschatz U 1990 *Pure & Appl. Chem*. **62** 1667.

[19] Gellert B and Kogelschatz U 1991 *Appl. Phys*. B **52** 14.

[20] Kogelschatz U 1992 *Appl. Surf. Sci*. **54** 410.

[21] Mildren R P and Carman R J 2001 *J. Phys. D: Appl. Phys*. **34** L1.

[22] Carman R J, Mildren R P, Ward B K and Kane D M 2004 *J. Phys. D: Appl. Phys*. **37** 2399.

[23] Oda A, Sugawara H, Sakai Y and Akashi H 2000 *J. Phys. D: Appl. Phys*. **33** 1507.

[24] Bogdanov E A, Kudryavtsev A A, Arslanbekov R R and Kolobov V I 2004 J. Phys. D: Appl. Phys. **37** 2987.

[25] Zhang J Y and Boyd I W 2000 Appl. Surf. Sci. **168** 296.

[26] Kogelschatz U, Eliasson B and Egli W 1997 *J. Phys. IV*, France, **7** C**4** 47.

[27] Yokatani A, Takezoe N, Kurosawa K, Igarashi T, and Matsuno H 1996 *Appl. Phys. Lett*. **69** 1399.

[28] Braun A M, Maurette M T and Oliveros E 1991 in *Photochemical Technology*, John Wiley & Sons, New York.

[29] Scheir R F and Fencl B F 1996 *Heat. Pip. Air Cond. J*. **68** 109.

[30] Elliott D J 1986 *Microlithography: Process Technology for IC Fabrication*, New York : McGraw-Hill.

[31] Collier D and Pantley W 1998 *Laser Focus World* **34** 63.

[32] Scheytt H, Esron H, Prager L, Mehnert R and Von Sonntag C 1993 in *Proceedings of the NATO Advanced Research Workshop on Non-Thermal Plasma Techniques for Pollution Control, Part B,* edited by P. Penetrante P and S. Schulthesis S, Springer-Verlag, Berlin, p. 91.

[33] Legrini O, Oliveros E, and Braun A M 1993 *Chem. Rev*. **93** 671.

[34] Sosnin E A, Oppenlander T and Tarasenko V F 2006 *Journal of Photochemistry and Photobiology* C**7** 145.

[35] Guivan N N, Janča J, Brablec A, Stáhel P, Slavíček P and Shimon L L 2005 *J. Phys. D: Appl. Phys*. **38** 3188.

[36] Avdeev S M, Boichenko A M, Sosnin E A, Tarasenko V F and Yakovlenko S I 2007 *Laser Physics* **17** 1119.

[37] Zhang J Y and Boyd I W 1996 *J. Appl. Phys*. **80** 633.

[38] Zhang J Y and Boyd I W 1998 *J. Appl. Phys*. **84** 1174.

[39] Falkenstein Z and Coogan J J 1997 *J. Phys. D: Appl. Phys*. **30** 2704.

[40] Merbahi N, Sewraj N, Marchal F, Salamero Y and Millet P 2004 *J. Phys. D: Appl. Phys*. **37** 1664.

[41] Oppenländer T, Potentials and Applications of Excimer Lamps (Incoherent Vacuum-UV/UV Sources) in *Photochemistry and in Photochemical Technology*, www.fh-furtwangen.de/deutsch/forschung/iaf/mitarbeiter/oppenlaender.html

[42] Kogelschatz U, Eliasson B and Egli W 1997, Invited paper ICPIG, Toulouse, France ; *J. Phys. IV*, Colloque C4, France C**4** 47.

[43] Kolts J H and Setser D W 1978 *J. Chem. Phys*. **68** 4848.

[44] Urakabe T, Harada S, Saikatsu T and Karino M 1996 *J. Light and Vis. Env*. **20** 20.

[45] Beaudette T, Guillot P, Belenguer P, Callegari T, Auday G 2006, Experimental Characterization of Dielectric Barrier Discharges for Mercury free Flat Lamp, in *XVIIIth Europhysics Conference on Atomic and Molecular Physics of Ionized Gases*, Lecce, Italia, July 12-16, p. 317.

[46] Beleznai Sz, Mihajlik G, Agod A, Maros I, Juhász R, Németh Zs, Jakab L and Richter P 2006, *J. Phys. D: Appl. Phys*. **39** 3777.

[47] Oda A, Sakai Y, Akashi H and Sugawara H 1999 *J. Phys. D: Appl. Phys*. **32** 2726.

[48] Liu S and Neiger M 2003 *J. Phys. D: Appl. Phys*. **36** 3144.

[49] Carman R J and Mildren R P 2003 *J. Phys. D: Appl. Phys*. **36** 19.

[50] Carman R J and Mildren R P 2002 *IEEE Trans. Plasma Sci*. **30** 154.

[51] Bogdanov E A, Kudryavtsev A A and Arslanbekov R R 2006 *Contrib. Plasma Phys*. **46** 807.

[52] Kwak M G, Han J I, Kim Y H, Park S K, Lee D K and Sohn S H 2003 *IEEE Trans. Plasma Sci*. **31**. 176.

[53] Adler F and Müller S 2000 *J. Phys. D: Appl. Phys*. **33** 1705.

[54] Shiga T, Pitchford L C, Boeuf J P, and Mikoshiba S 2003 *J. Phys. D: Appl. Phys*. **36** 512.

[55] Kwak M G and Han J I 2001 *J. SID* **9** 165.

[56] Jing-zhou X, Wei L, Rong-qing L and Zhao-xing R 2001 *Plasma Science and Technology* **3** 1027.

[57] Belasri A, Boeuf J P and Pitchford L C 1993 *J. Appl. Phys*.**74** 1553.

[58] Belasri A, Bendella S and Baba-Hamed T 2008 *Physics of Plasmas* **15** 053502.

[59] Gear C W 1971, *Numerical Initial Value Problems in Ordinary Differential Equations*, Prentice-Hall, Englewood Cliffs, NJ.

[60] Meunier J, Belenguer P and Boeuf J P 1995 *J. Appl. Phys*. **78** 731.

[61] Ouyang J, He F, Miao J, Wang J and Hu W 2007 *J. Appl. Phys*. **101** 043303.

[62] BOLSIG+, KINEMA Software, [On-line]: http://www.siglo-kinema.com

[63] Levin L A, Moody S E, Klosterman B L, Center R E and Ewing J J 1981 *IEEE J. Quantum Electron*. QE-**17** 2282 .

[64] Oskam H J and Mittelstadt V R 1963 *Phys. Rev*. **32** 1445.

[65] Inoue G, Ku J K and Setser D W 1984 *J. Chem. Phys*. **81** 5760.

[66] Galy J, Aouame K, Birot A, Brunet H and Millet P 1993 *J. Phys*. B **26** 447.

[67] Salamero Y, Birot A, Galy J and Millet P 1984 *J. Chem. Phys*. **80** 4774.

[68] Brodmann R and Zimmerer G 1977 *J. Phys. B* **10** 3395.

[69] Alford W J 1992 *J. Chem. Phys*. **96** 4330.

[70] Keto J W, Gleason R E, Bomifield J D, Walters G K and Soley E K 1976 *Chem. Phys. Lett*. **42** 125.

[71] Thornton G, Poliakoff E D, Matthias E, Southworth S H, Rosenberg R A, White M G and Shirley D A 1979 *J. Chem. Phys*. **71** 133.

[72] Callegari T 2000, PhD Thesis – University Paul Sabatier of Toulouse, France.

[73] Hirech A 1997, PhD Thesis – University Paul Sabatier of Toulouse, France.

[74] Beaudette T 2009, PhD Thesis – University Paul Sabatier of Toulouse, France.

[75] Boeuf J P 2003 *J. Phys. D : Appl. Phys*. **36** R53.

List of tables

Table 1.

NO.	Reaction	Rate constant	Reference
Direct ionization			
R1	$e + Xe \rightarrow Xe^{+} + 2e$	Tabled	[62]
R2	$e + Ne \rightarrow Ne^{+} + 2e$	Tabled	[62]
Excitation			
R3	$e + Xe \rightarrow Xe^{*}(^{3}P_{2}) + e$	Tabled	[62]
R4	$e + Xe \rightarrow Xe^{*}(^{3}P_{1}) + e$	Tabled	[62]
R5	$e + Ne \rightarrow Ne^{*} + e$	Tabled	[62]
R6	$e + Xe \rightarrow Xe^{**} + e$	Tabled	[62]
Stepwise ionization			
R7	$e + Xe^{*}(^{3}P_{2}) \rightarrow Xe^{+} + 2e$	Tabled	[62]
R8	$e + Ne^{*} \rightarrow Ne^{+} + 2e$	Tabled	[62]
Penning ionization			
R9	$Ne^{*} + Xe \rightarrow Ne + Xe^{+} + e$	7.5×10^{-11} $cm^{3} s^{-1}$	[63]
R10	$Ne^{*} + Xe \rightarrow NeXe^{+} + e$	2.3×10^{-11} $cm^{3} s^{-1}$	[63]
Three–body collisions			
R11	$Ne^{+} + 2Ne \rightarrow Ne_{2}^{+} + Ne$	4.4×10^{-32} $cm^{6}s^{-1}$	[63]
R12	$Ne^{+} + Xe + Ne \rightarrow NeXe^{+} + Ne$	1×10^{-31} $cm^{6}s^{-1}$	[63]
R13	$Xe^{+} + 2Ne \rightarrow NeXe^{+} + Ne$	1×10^{-31} $cm^{6}s^{-1}$	[63]
R14	$Xe^{+} + 2Xe \rightarrow Xe_{2}^{+} + Xe$	2.5×10^{-31} $cm^{6}s^{-1}$	[63]
R15	$Xe^{+} + Xe + Ne \rightarrow Xe_{2}^{+} + Ne$	1.5×10^{-31} $cm^{6}s^{-1}$	[63]
Electron-ion recombination			
R16	$Ne_{2}^{+} + e \rightarrow Ne^{*} + Ne$	$3.7\times10^{-8}\times T_{e}^{-0.43}$ $cm^{3} s^{-1}$	[63]
R17	$Xe_{2}^{+} + e \rightarrow Xe^{**} + Xe$	$2\times10^{-7}\times T_{e}^{-0.5}$ $cm^{3} s^{-1}$	[64]
R18	$NeXe^{+} + e \rightarrow Xe^{**} + Ne$	$8\times10^{-8}\times T_{e}^{-0.5}$ $cm^{3} s^{-1}$	[63]
Charge exchange			
R19	$NeXe^{+} + Xe \rightarrow Xe^{+} + Ne + Xe$	5×10^{-10} $cm^{3} s^{-1}$	[63]
R20	$NeXe^{+} + Xe \rightarrow Xe_{2}^{+} + Ne$	5×10^{-12} $cm^{3} s^{-1}$	[63]
Neutral kinetics			
R21	$Xe^{**} + Ne \rightarrow Xe^{*}(^{3}P_{2}, {}^{3}P_{1}) + Ne$	2×10^{-12} $cm^{3} s^{-1}$	[65]
R22	$Xe^{**} + Xe \rightarrow Xe^{*}(^{3}P_{2}, {}^{3}P_{1}) + Xe$	1×10^{-10} $cm^{3} s^{-1}$	[65]
R23	$Xe^{*}(^{3}P_{1}) + Ne \rightarrow Xe^{*}(^{3}P_{2}) + Ne$	3.1×10^{-14} $cm^{3} s^{-1}$	[66]
R24	$Xe^{*}(^{3}P_{2}) + Ne \rightarrow Xe^{*}(^{3}P_{1}) + Ne$	1.62×10^{-16} $cm^{3} s^{-1}$	[66]
R25	$Xe^{*}(^{3}P_{1}) + Xe \rightarrow Xe^{*}(^{3}P_{2}) + Xe$	2.18×10^{-14} $cm^{3} s^{-1}$	[67]
R26	$Xe^{*}(^{3}P_{2}) + Xe \rightarrow Xe^{*}(^{3}P_{1}) + Xe$	1.26×10^{-16} $cm^{3} s^{-1}$	[67]
R27	$Xe^{*}(^{3}P_{1}) + 2Xe \rightarrow Xe_{2}^{*}(O_{u}^{+}) + Xe$	1.55×10^{-31} $cm^{6} s^{-1}$	[66]
R28	$Xe^{*}(^{3}P_{2}) + 2Xe \rightarrow Xe_{2}^{*}(^{3}\Sigma_{u}^{+}) + Xe$	8.53×10^{-32} $cm^{6} s^{-1}$	[66]
R29	$Xe^{*}(^{3}P_{1}) + Xe + Ne \rightarrow Xe_{2}^{*}(O_{u}^{+}) + Ne$	4.07×10^{-32} $cm^{6} s^{-1}$	[66]
R30	$Xe^{*}(^{3}P_{2}) + Xe + Ne \rightarrow Xe_{2}^{*}(^{3}\Sigma_{u}^{+}) + Ne$	1.35×10^{-32} $cm^{6} s^{-1}$	[66]
R31	$Xe_{2}^{*}(O_{u}^{+}) + Xe \rightarrow Xe_{2}^{*}(^{1}\Sigma_{u}^{+}) + Xe$	2.6×10^{-10} $cm^{3} s^{-1}$	[68]
Spontaneous emissions			
R32	$Xe^{**} \rightarrow Xe^{*}(^{3}P_{2}, {}^{3}P_{1}) + h\upsilon$	3×10^{7} s^{-1}	[69]
R33	$Xe^{*}(^{3}P_{1}) \rightarrow Xe + h\upsilon(147\ nm)$	2.7×10^{6} s^{-1}	[66]
R34	$Xe_{2}^{*}(^{1}\Sigma_{u}^{+}) \rightarrow 2Xe + h\upsilon(173\ nm)$	5×10^{8} s^{-1}	[70]
R35	$Xe_{2}^{*}(^{3}\Sigma_{u}^{+}) \rightarrow 2Xe + h\upsilon(173\ nm)$	1.66×10^{8} s^{-1}	[69]
R36	$Xe_{2}^{*}(O_{u}^{+}) \rightarrow 2Xe + h\upsilon(150\ nm)$	9×10^{6} s^{-1}	[71]

Table 2.

Parameter	**Value**
Gas mixture Ne–Xe	10, 20, 30% of xenon in neon.
Gas pressure	p_r= 300, 400, 600 Torr
Gas temperature	T_g= 300 °K
Gap length	d= 5 mm
Cathode region length	d_{cr}= 3 mm
Electrode area	A= 1 cm^2
Applied voltage	V_{ap}= 1.5, 2, 3 kV
Dielectric capacitance	C_{diel}= 100, 230, 400 pF/cm^2
Coefficient of secondary emission	γ = 0.1, 0.25
Initial electron density	10^9 cm^{-3}

Figures list

Figure 1

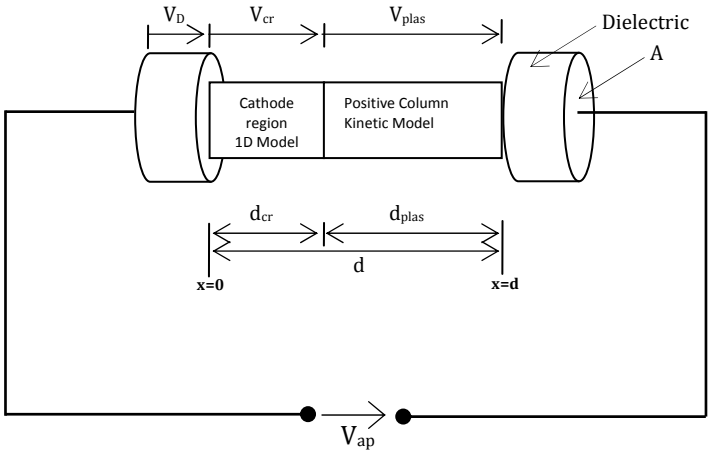
V_D
V_{cr}
V_{plas}
Dielectric
A
Cathode region 1D Model
Positive Column Kinetic Model
d_{cr}
d_{plas}
d
x=0
x=d
V_{ap}

Figure 2

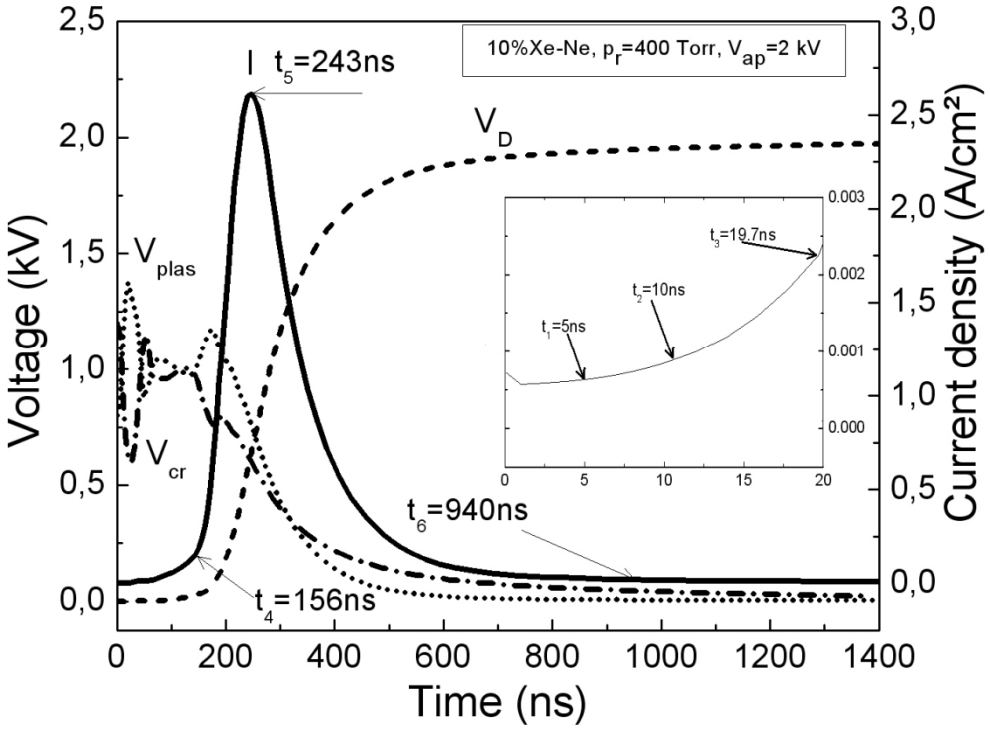
10%Xe-Ne, p_r=400 Torr, V_ap=2 kV
I
t_5=243ns
V_D
V_plas
V_cr
t_6=940ns
t_4=156ns
t_1=5ns
t_2=10ns
t_3=19.7ns
Voltage (kV)
Current density (A/cm²)
Time (ns)
0,0
0,5
1,0
1,5
2,0
2,5
3,0
0
200
400
600
800
1000
1200
1400
0.000
0.001
0.002
0.003
5
10
15
20

Figure 3

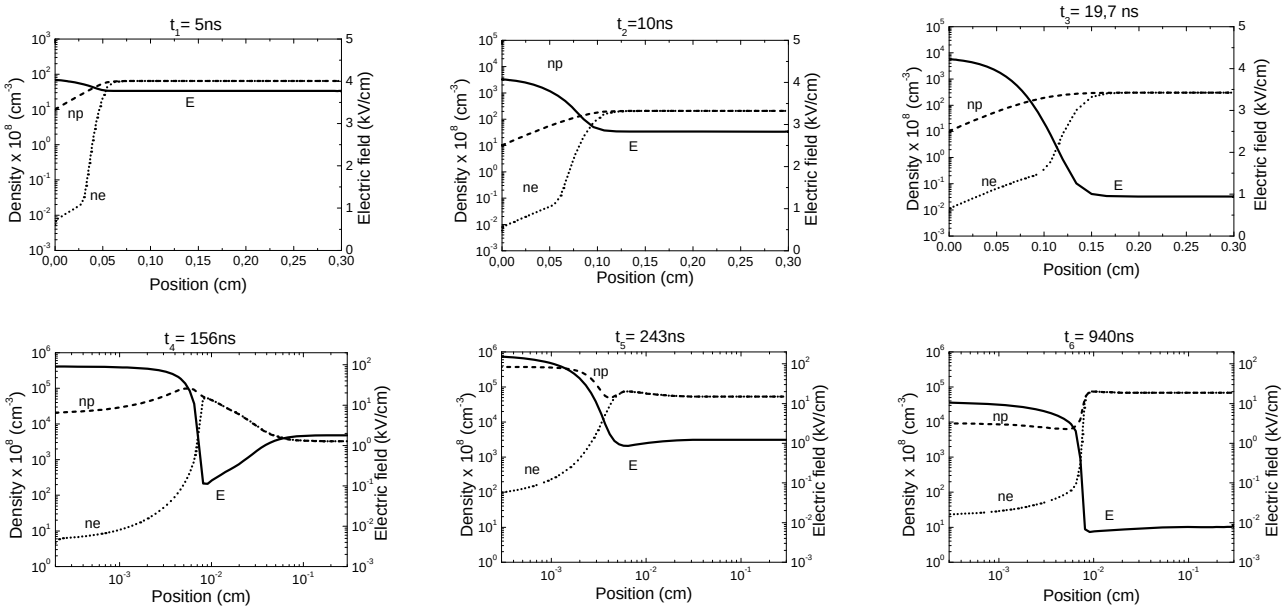
t1= 5ns
t2=10ns
t3= 19,7 ns
t4= 156ns
t5= 243ns
t6= 940ns
np
ne
E
Density x 10^8 (cm^-3)
Electric field (kV/cm)
Position (cm)

Figure 4

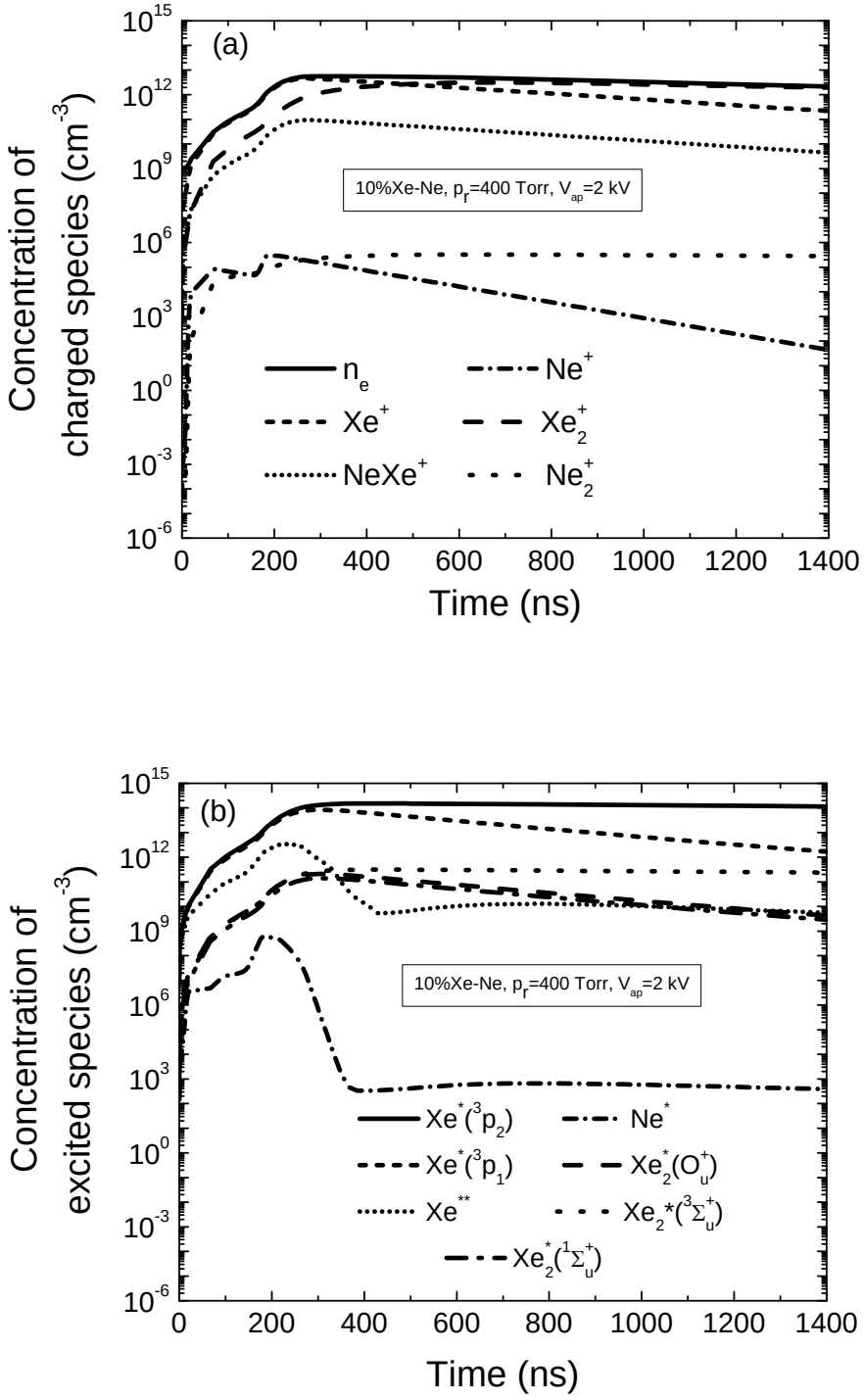
(a)
10%Xe-Ne, p_r=400 Torr, V_ap=2 kV
Concentration of charged species (cm^-3)
Time (ns)
n_e
Ne+
Xe+
Xe2+
NeXe+
Ne2+
(b)
10%Xe-Ne, p_r=400 Torr, V_ap=2 kV
Concentration of excited species (cm^-3)
Time (ns)
Xe*(3p2)
Ne*
Xe*(3p1)
Xe2*(Ou+)
Xe**
Xe2*(3Σu+)
Xe2*(1Σu+)

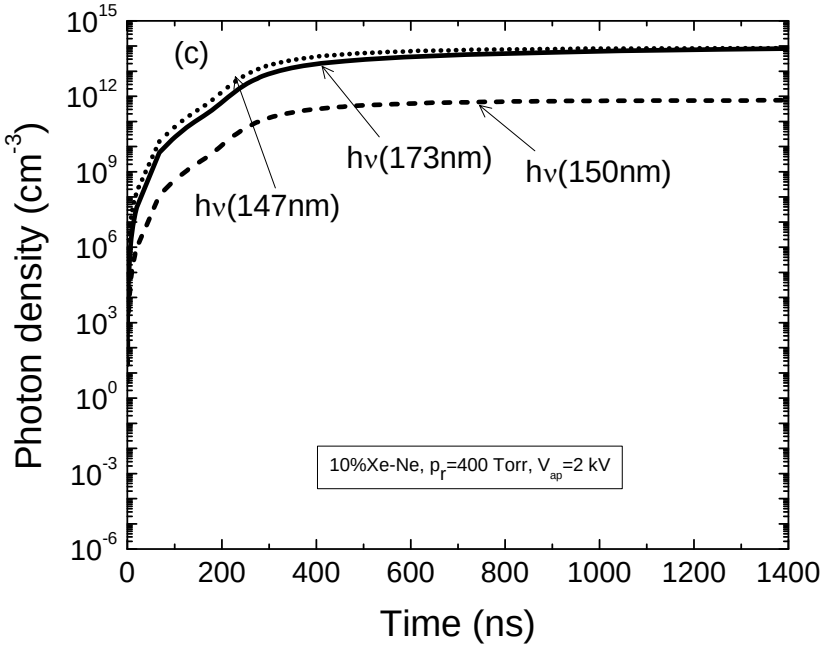
(c)
hν(147nm)
hν(173nm)
hν(150nm)
10%Xe-Ne, p_r=400 Torr, V_ap=2 kV
Photon density (cm^-3)
Time (ns)
10^15
10^12
10^9
10^6
10^3
10^0
10^-3
10^-6
0
200
400
600
800
1000
1200
1400

Figure 5

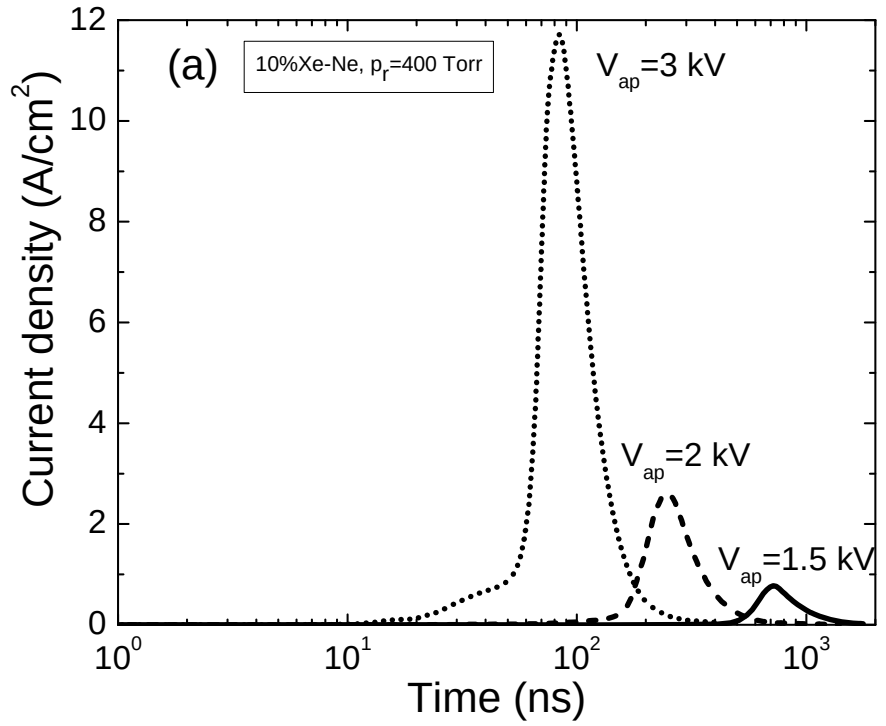
(a)
10%Xe-Ne, p_r=400 Torr
V_ap=3 kV
V_ap=2 kV
V_ap=1.5 kV
Current density (A/cm^2)
Time (ns)
0
2
4
6
8
10
12
10^0
10^1
10^2
10^3

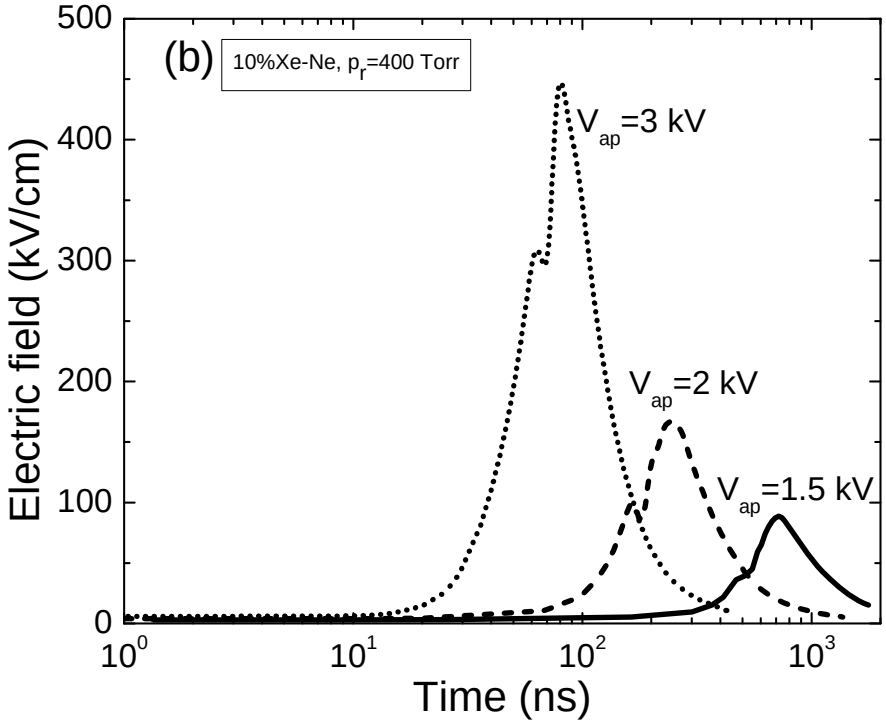
(b)
10%Xe-Ne, p_r=400 Torr
V_ap=3 kV
V_ap=2 kV
V_ap=1.5 kV
Electric field (kV/cm)
Time (ns)
0
100
200
300
400
500
10^0
10^1
10^2
10^3

Figure 6

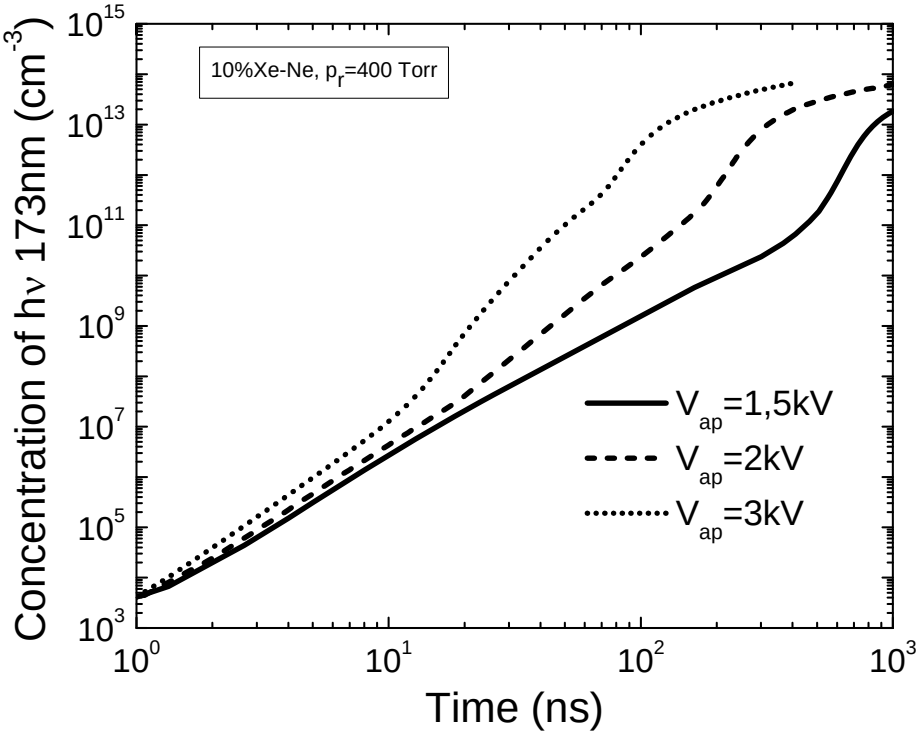
10%Xe-Ne, p_r=400 Torr
V_ap=1,5kV
V_ap=2kV
V_ap=3kV
Concentration of hν 173nm (cm^-3)
Time (ns)
10^15
10^13
10^11
10^9
10^7
10^5
10^3
10^0
10^1
10^2
10^3

Figure 7

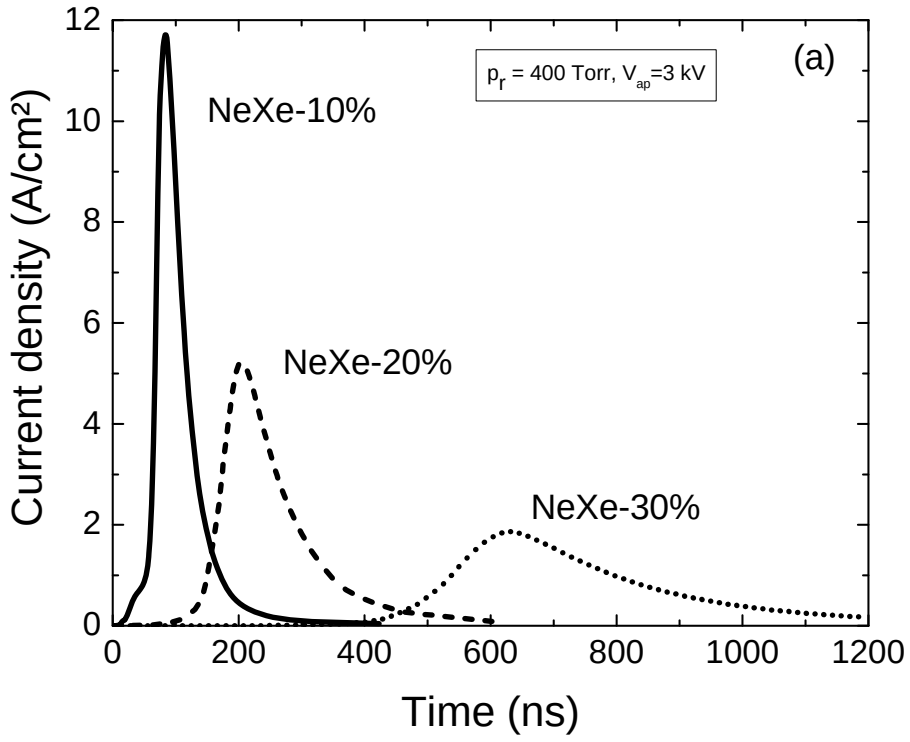
(a)
p_r = 400 Torr, V_{ap}=3 kV
NeXe-10%
NeXe-20%
NeXe-30%
Current density (A/cm²)
Time (ns)
0
2
4
6
8
10
12
0
200
400
600
800
1000
1200

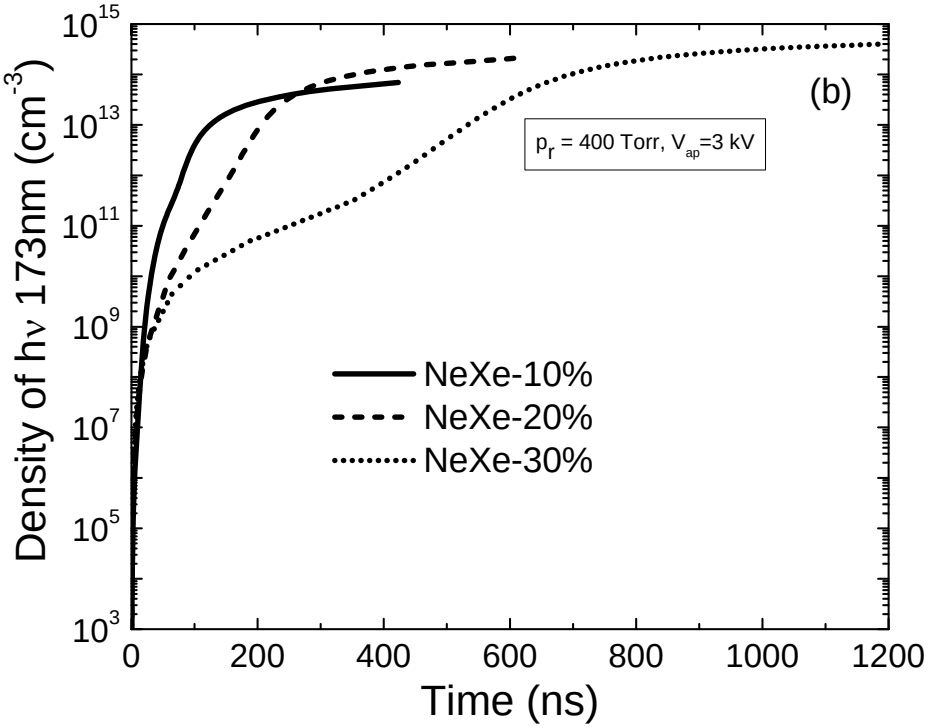
(b)
p_r = 400 Torr, V_{ap}=3 kV
NeXe-10%
NeXe-20%
NeXe-30%
Density of hν 173nm (cm^{-3})
Time (ns)
10^{3}
10^{5}
10^{7}
10^{9}
10^{11}
10^{13}
10^{15}
0
200
400
600
800
1000
1200

Figure 8

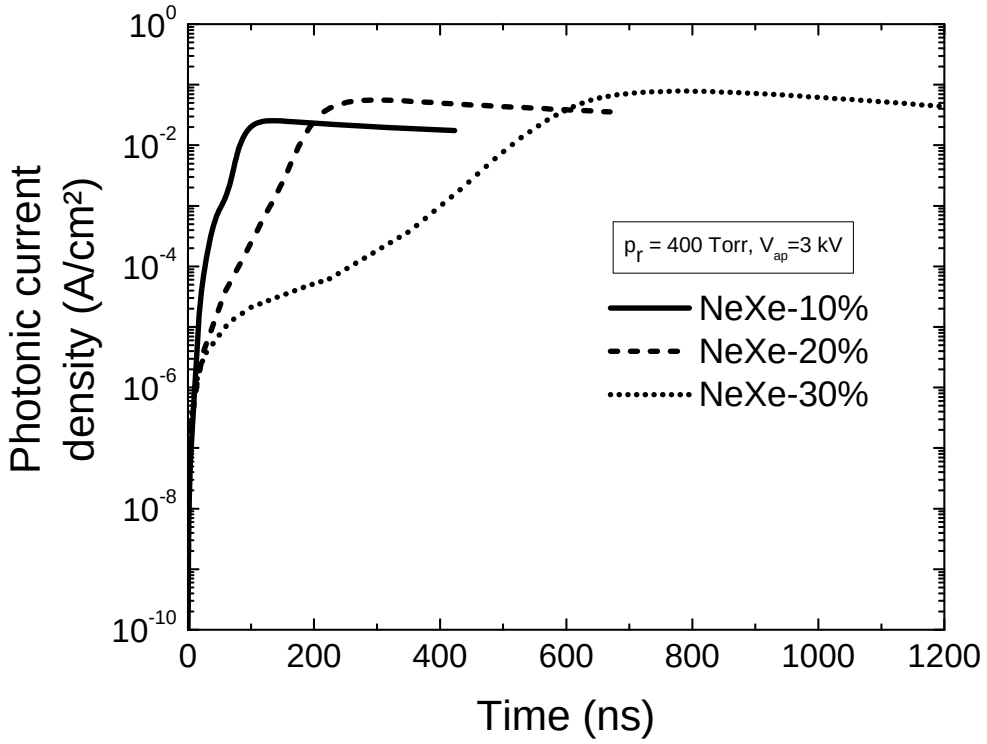
Photonic current density (A/cm²)
Time (ns)
p_r = 400 Torr, V_ap=3 kV
NeXe-10%
NeXe-20%
NeXe-30%
10^0
10^-2
10^-4
10^-6
10^-8
10^-10
0
200
400
600
800
1000
1200

Figure 9

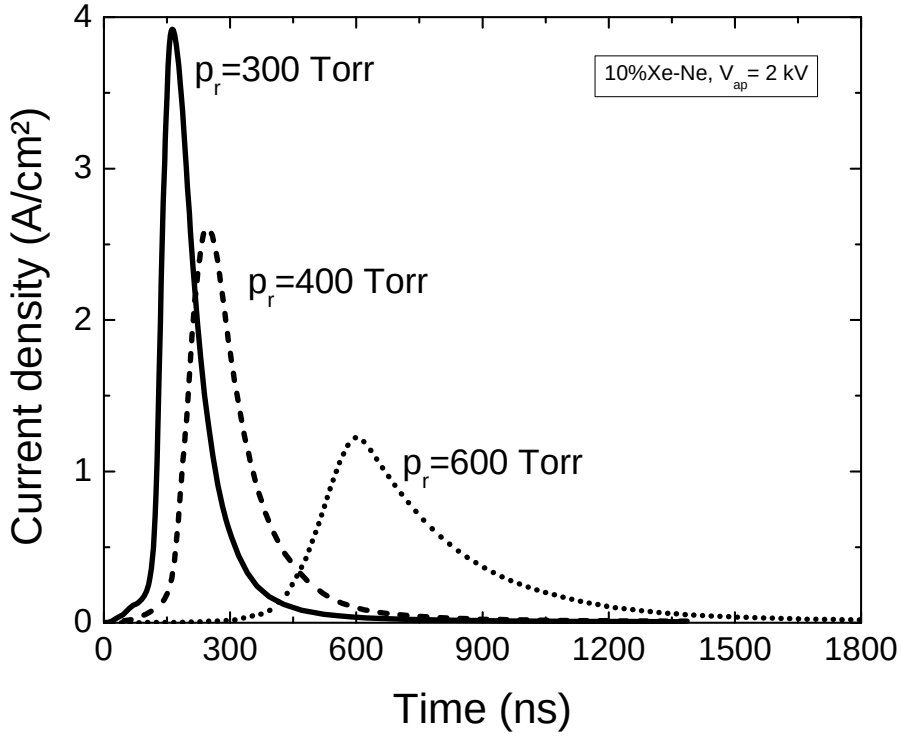
Current density (A/cm²)
Time (ns)
p_r=300 Torr
p_r=400 Torr
p_r=600 Torr
10%Xe-Ne, V_ap = 2 kV
0
1
2
3
4
0
300
600
900
1200
1500
1800

Figure 10

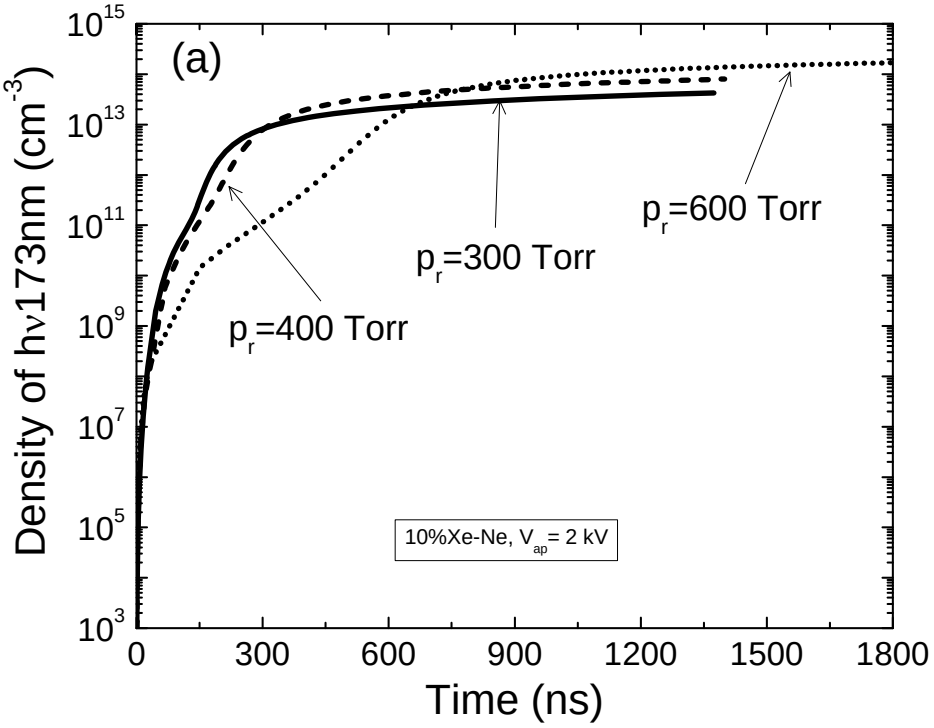
(a)
Density of hν173nm (cm-3)
Time (ns)
pr=600 Torr
pr=300 Torr
pr=400 Torr
10%Xe-Ne, Vap= 2 kV

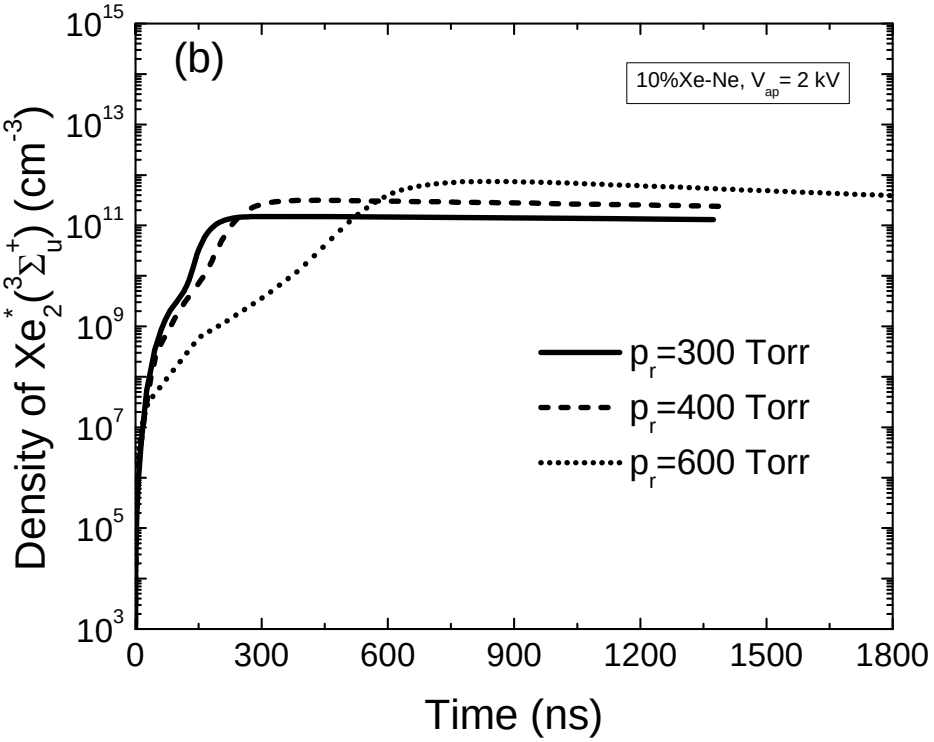
(b)
Density of Xe2*(3Σu+) (cm-3)
Time (ns)
10%Xe-Ne, Vap= 2 kV
pr=300 Torr
pr=400 Torr
pr=600 Torr

Figure 11

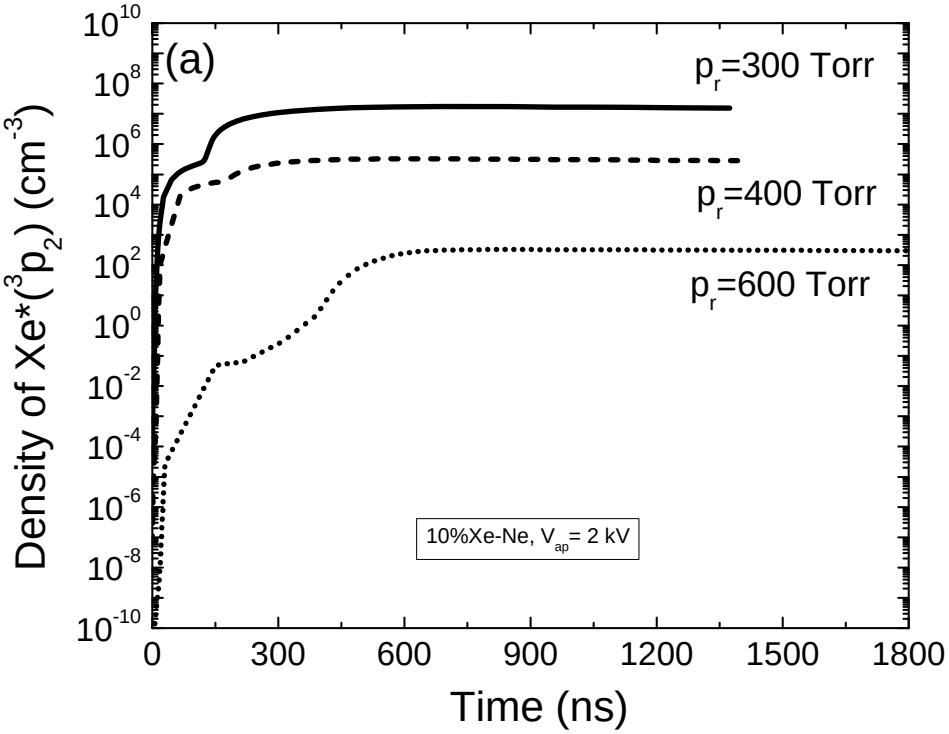
(a)
p_r=300 Torr
p_r=400 Torr
p_r=600 Torr
10%Xe-Ne, V_ap= 2 kV
Density of Xe*(3p2) (cm-3)
Time (ns)

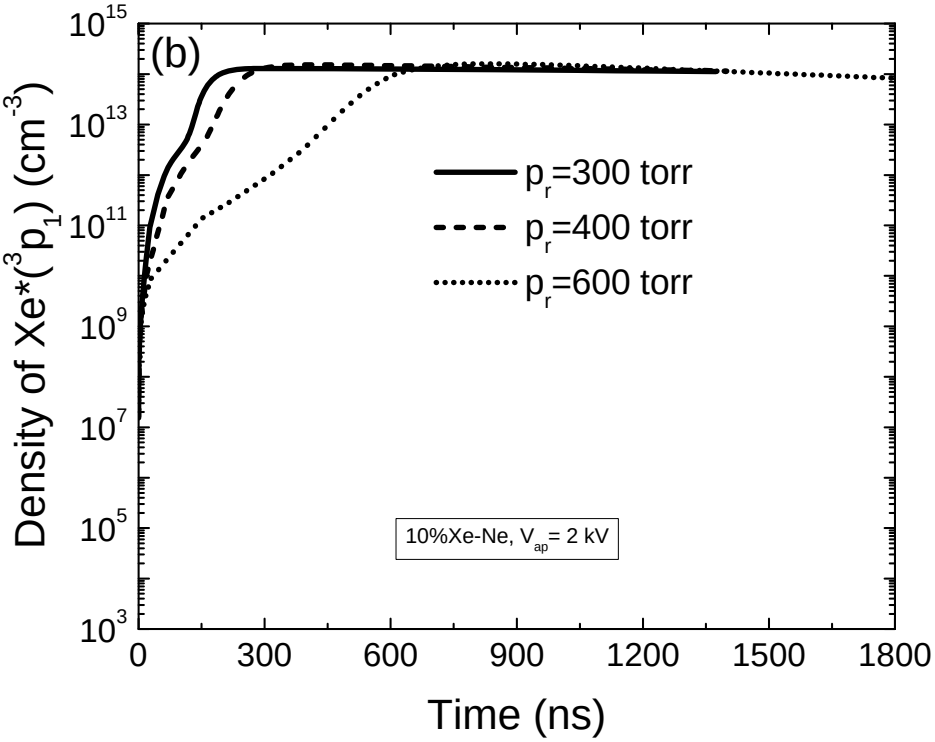
(b)
p_r=300 torr
p_r=400 torr
p_r=600 torr
10%Xe-Ne, V_ap= 2 kV
Density of Xe*(3p1) (cm-3)
Time (ns)

Figure 12

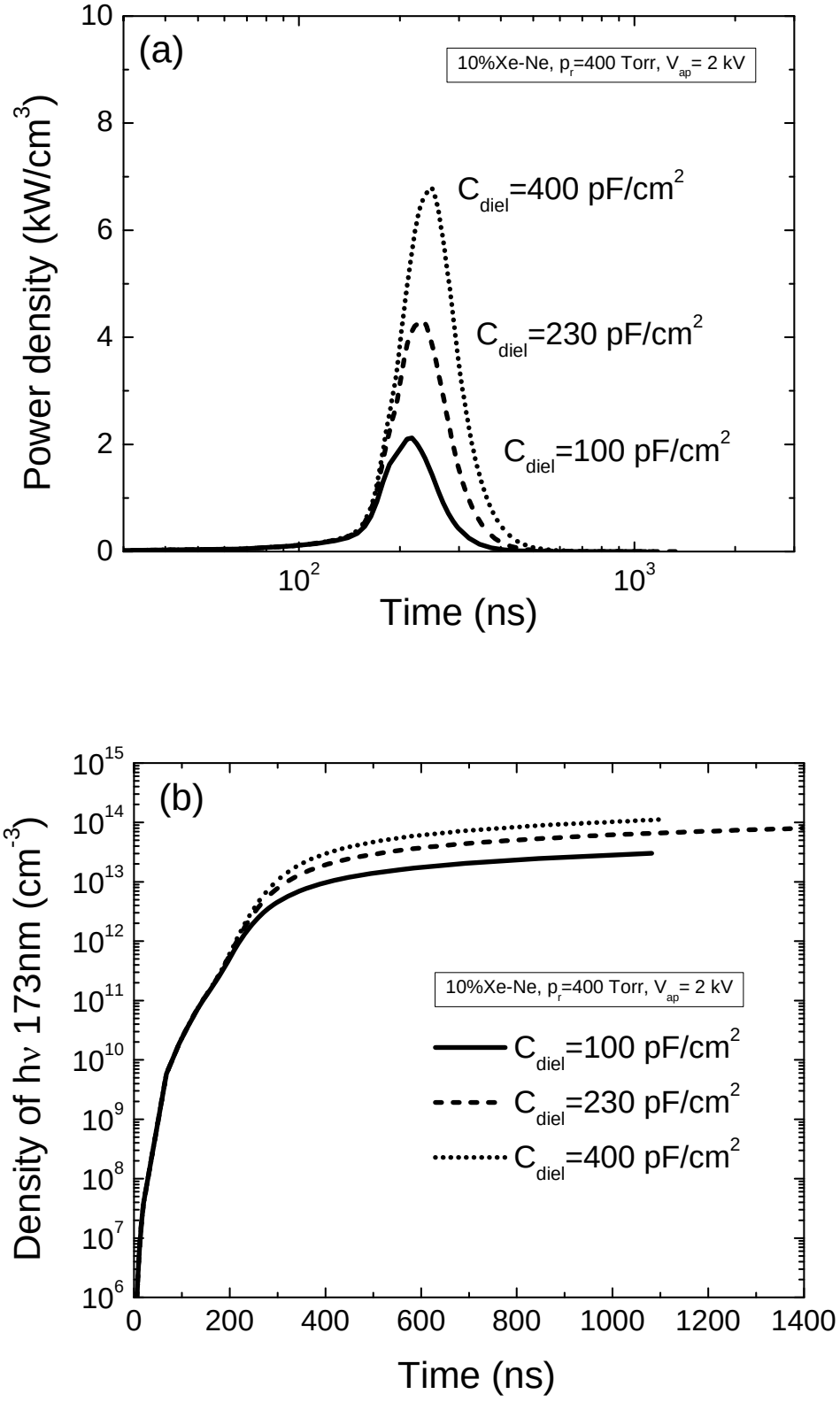
(a)
10%Xe-Ne, p_r=400 Torr, V_ap= 2 kV
C_diel=400 pF/cm^2
C_diel=230 pF/cm^2
C_diel=100 pF/cm^2
Power density (kW/cm^3)
Time (ns)
(b)
10%Xe-Ne, p_r=400 Torr, V_ap= 2 kV
C_diel=100 pF/cm^2
C_diel=230 pF/cm^2
C_diel=400 pF/cm^2
Density of hν 173nm (cm^-3)
Time (ns)

Figure 13

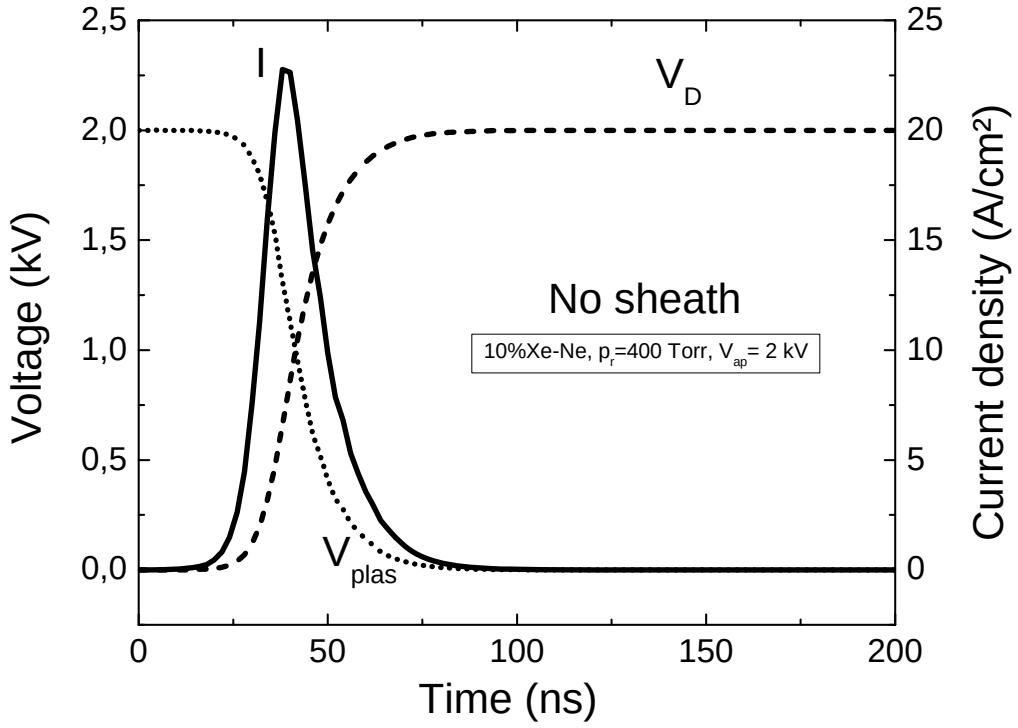
2,5
2,0
1,5
1,0
0,5
0,0
25
20
15
10
5
0
0
50
100
150
200
Time (ns)
Voltage (kV)
Current density (A/cm²)
I
V_D
V_plas
No sheath
10%Xe-Ne, p_r=400 Torr, V_ap= 2 kV

Figure 14

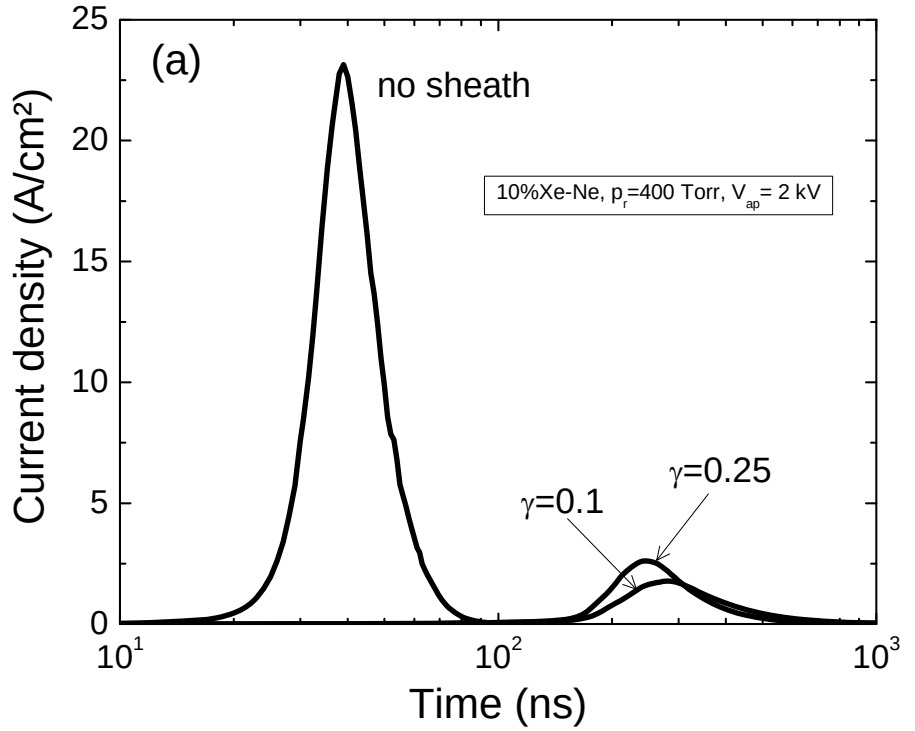
(a)
no sheath
10%Xe-Ne, p_r=400 Torr, V_ap= 2 kV
γ=0.1
γ=0.25
Current density (A/cm²)
Time (ns)

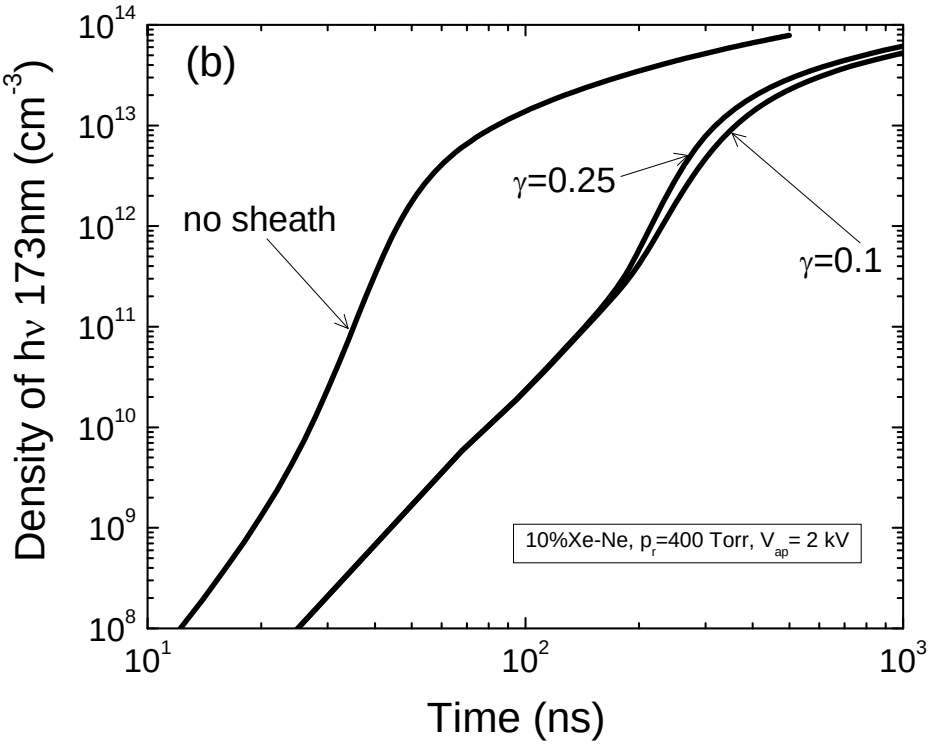
(b)
no sheath
γ=0.25
γ=0.1
10%Xe-Ne, p_r=400 Torr, V_ap= 2 kV
Density of hν 173nm (cm^-3)
Time (ns)